Journal of Marine Research, 50, 441–463, 1992

Modelling the deep-chlorophyll maximum: A coupled physical-biological approach

by Ramiro A. Varela,[1] Antonio Cruzado,[1] Joaquín Tintoré[2] and Emilio García Ladona[3]

ABSTRACT

The Deep Chlorophyll Maximum (DCM) is simulated in two oligotrophic regions (SW Sargasso Sea and NW Mediterranean) using a physical/biological model that couples an upper ocean turbulent model to a nutrient/phytoplankton model. The biological model considers two types of primary producers, heterotrophs and atmospheric in addition to internal nitrate inputs. Model results appear to adequately reproduce the DCM structure in those regions. The DCM depth and magnitude is mainly determined by the vertical eddy diffusion and light extinction. The grazing parameters mainly affect the intensity of the DCM. This suggest the DCM is primarily the result of a balance between upward nutrient flux and light field characteristics. Consequently, the regenerated production only plays a secondary role.

1. Introduction

Significant regions of the world's oceans, from the North Atlantic and Pacific gyres to the Mediterranean Sea, show oligotrophic conditions during the period of vertical stratification. In such areas, however, a deep chlorophyll maximum (DCM) is frequently observed below the thermocline.

Since the early studies on the DCM (Riley, 1949; Steele and Yentsch, 1960) a large amount of scientific effort has been directed to the understanding of such a feature. The significance of the DCM cannot be overemphasized since even though it is highly variable in depth and magnitude, it can account for a significant fraction of the total primary production in the water column (Takahashi and Hori, 1984).

Different theories have been advanced to explain this phenomenon. Strictly biological arguments were given by Anderson (1969) who suggested that the DCM originates from photosynthetically active phytoplankton populations adapted to low light intensities. Herbland (1983) related the DCM structure to the nutrient vertical distribution and to a phytoplankton biomass maximum. Takahashi and Hori (1984) among others, related the appearance of the DCM to a decrease in the sinking rate of the nutrient-impoverished cells. More recently, Taguchi *et al.* (1988) suggested

1. Centre d'Estudis Avançats de Blanes, 17300 Blanes-Girona, Spain.
2. Dept. de Física, Universitat de les Illes Balears, 07071 Palma de Mallorca, Spain.
3. Dept. de Física, Universitat Autónoma de Barcelona, 08193 Bellaterra (Barcelona), Spain.

that at low light levels, the DCM is the result of higher chlorophyll cellular content rather than a real increase of phytoplankton biomass.

Other studies have related the existence of the DCM to coupled physical/biological processes. Banse (1987) related the DCM and the associated nutricline to atmospheric conditions and mixed layer depth. He pointed out that, when the DCM is located in the top of the pycnocline, cloudiness can enhance the nutrient flux into the mixed layer. Flos and Tintoré (1990) suggested that the DCM patterns observed off the northeast Spanish coast (Estrada and Salat, 1989) were related to mesoscale instabilities of the shelf/slope front.

Numerical modelling studies have also been carried out to estimate nutrient fluxes and phytoplankton distribution. Initially, most of these studies emphasized the biological processes using simplified physics. Wroblewski and O'Brien (1976) parameterized turbulent diffusion with constant vertical eddy coefficients. Jamart *et al.* (1977) used a two layer model with a depth-dependent eddy coefficient to simulate the subsurface chlorophyll maximum in the offshore Pacific waters.

Kiefer and Kremer (1981) used a mixed layer model (Gill and Turner, 1976) to study the origin of the vertical distribution of phytoplankton in temperate oceans. They showed that the DCM is mainly determined by the dynamics of the seasonal thermocline. In other words, they recognized that mixed layer dynamics influence the supply of nutrients from below the thermocline and therefore strongly affect the DCM formation and maintenance.

More recent studies considered more complex physics but with simplified biology. Klein and Coste (1984) used a second order turbulent closure and showed the influence of transient wind driven mixed layer deepening on the upward nutrient flux. Chen *et al.* (1988) used a similar type of model and studied the combined effects of wind and tidal mixing on the vertical nutrient fluxes. Holloway and Denman (1989) showed the influence of internal waves on primary production, a process not included in previous studies.

All these previous studies have therefore showed that it is essential to include the relevant physical and biological processes to understand nutrient fluxes and the DCM structure in the water column. The goal of this work is to analyze the different physical and biological processes that determine the existence of a DCM using a sophisticated physical/biological model. In essence an upper ocean turbulent closure model has been coupled to a general nutrient/phytoplankton model. Results are compared with data from two oligotrophic areas, the Sargasso Sea and the northwestern Mediterranean. Finally, our findings are discussed from the standpoint of the deep chlorophyll maximum. In a separate manuscript we will present a detailed sensitivity analysis where the role of several physical and biological processes on the DCM structure is analyzed in detail.

2. The physical model

a. Description. The mixed layer structure has been simulated using a one dimensional *k-model* (Mellor and Yamada, 1974). This kind of model gives an accurate

estimate of eddy coefficients with moderate computing cost (Gaspar *et al.*, 1988). Assuming no horizontal variability, the horizontal momentum equations in an (x, y, z) reference frame are:

$$\frac{\partial u}{\partial t} - fv = \frac{\partial}{\partial z}\left[\tilde{\nu}\frac{\partial u}{\partial z}\right] \tag{1}$$

$$\frac{\partial v}{\partial t} - fu = \frac{\partial}{\partial z}\left[\tilde{\nu}\frac{\partial v}{\partial z}\right] \tag{2}$$

where t is time, u and v are the horizontal velocities, f is the Coriolis parameter and $\tilde{\nu}$ is the eddy viscosity. The evolution of the thermodynamic variables is written in a conservative way as,

$$\frac{\partial T}{\partial t} = \frac{\partial}{\partial z}\left[\lambda_t \frac{\partial T}{\partial z}\right] \tag{3}$$

$$\frac{\partial S}{\partial t} = \frac{\partial}{\partial z}\left[\lambda_s \frac{\partial S}{\partial z}\right] \tag{4}$$

$$\rho = \rho(T, S) \tag{5}$$

where T, S and ρ are the temperature, salinity and density respectively. Density was calculated from temperature and salinity by means of the seawater state equation given by Millero and Poisson (1981). λ's are the heat and salt diffusivities also functions of z and t. In the following, the assumption is made that $\lambda_s = \lambda_t$ and the notation will be λ.

Since the vertical eddy viscosities and diffusivities are unknown, to close these equations we have two possibilities (Rodi, 1987). One is to provide eddy coefficients as empirical functions of known average variables. The other possibility is to compute these coefficients as functions of the turbulent kinetic energy (k) and the mixing length (l_m, e.g. Mellor and Yamada, 1974):

$$\tilde{\nu} \approx \frac{1}{2}\sqrt{k}\, l_m. \tag{6}$$

Therefore, we need a new equation for the turbulent kinetic energy:

$$\frac{\partial k}{\partial t} = \tilde{\nu}\left\|\frac{\partial \mathbf{u}}{\partial z}\right\| - \lambda\frac{g}{\rho_0}\frac{\partial \rho}{\partial z} - \epsilon = \tilde{\nu}\left\|\frac{\partial \mathbf{u}}{\partial z}\right\|(1 - R_f) - \epsilon \tag{7}$$

where ϵ is viscous dissipation and R_f is the flux Richardson number:

$$R_f = \frac{\lambda}{\tilde{\nu}} R_i \tag{8}$$

where R_i is the Richardson number.

$$R_i = \frac{N^2}{\left(\frac{\partial u}{\partial z}\right)^2 + \left(\frac{\partial v}{\partial z}\right)^2} \qquad \text{with } N^2 \equiv -\frac{g}{\rho}\frac{\partial \rho}{\partial z}. \tag{9–10}$$

In Eq. (7) vertical diffusion of turbulent kinetic energy was not included, since this term becomes negligible when the turbulent kinetic energy flux at the surface is not considered. It is also generally assumed that dissipation is given by (Rodi, 1987):

$$\epsilon \approx \frac{k^2}{16\tilde{\nu}}. \tag{11}$$

A simplified model was used here by assuming that turbulent kinetic energy reaches local equilibrium values between shear production and dissipation ($\partial k/\partial z = 0$). As a result, the explicit dependence on the turbulent kinetic energy can be eliminated using (11), (6) and (7):

$$\tilde{\nu} = l_m^2 \left\| \frac{\partial \mathbf{u}}{\partial z} \right\|^{1/2} (1 - R_f)^{1/2} \tag{12}$$

where the mixing length is given by:

$$l_m = l_0(1 - R_f) \tag{13}$$

with

$$l_0 = kz\left[1 - \frac{z}{H}\right] \tag{14}$$

where H is the total depth and k is the Von Karman constant (roughly equal to 0.4).

Finally, the eddy diffusion is related to the eddy viscosity (Nihoul, 1982) by:

$$\lambda = \tilde{\nu}\gamma\sqrt{1 - R_f} \tag{15}$$

where λ is a parameter (e.g., $\lambda = 1.1$, Nihoul, 1982).

Then (1)–(5) and (12)–(15) form a closed set of differential equations which can solve the time dependent evolution of the mixed layer and provide the eddy coefficients to the biological model.

b. Initial and boundary conditions. The initial u and v velocities are set to zero, while the initial temperature and salinity profiles are taken from CTD casts. At the surface, wind stress is computed as:

$$\boldsymbol{\tau} = 0.63 \times 10^{-6}(1 + 0.1|\mathbf{u}_{10}|)|\mathbf{u}_{10}|\mathbf{u} \tag{16}$$

where $|\mathbf{u}_{10}| = \sqrt{(u_{10}^2 + v_{10}^2)}$ and u_{10} and v_{10} are the wind speed at 10 m height.

Surface heat flux was obtained as:

$$\lambda \left(\frac{\partial T}{\partial z}\right)_{z=0} = K(T_a - T_s) \tag{17}$$

where T_a and T_s are the air and sea temperature, and K is a heat exchange coefficient (e.g., 10^{-3}, Chen *et al.*, 1988). A no flux condition was considered for salinity.

At the bottom, no fluxes of salt or heat were considered, and since the modelled regions are always far from the shelf (actual depths greater than 1000 m, while our concern were the top 300 m), bottom friction was neglected.

The equations were solved with a semi-implicit finite-difference method, forward in time and centered in space. This method produces a tri-diagonal matrix which was solved by a standard algorithm. A 2 m vertical grid that produces 150 levels for a domain of 300 m depth was used, and the time step was 240 s to filter high frequency motions that could not be resolved by the model.

3. The biological model

a. Description and general assumptions. The biological model is based on the "classical" trophic food web scheme of Michaels and Silver (1988) and includes five variables: heterotrophs (H), small (P) and large (L) phytoplankton, and the major nitrogen nutrients (NO_3 and NH_4, see Fig. 1). The zooplankton (Z) is considered as a closure condition, and is estimated as a function of the heterotrophs and large phytoplankton. Particulate organic matter (POM) is also estimated from the available zooplankton and not explicitly modelled.

The building unit is nitrogen, which is generally assumed to be the main element in limiting the phytoplankton growth in oligotrophic seas.

Inorganic nitrogen in the model is assumed to be composed by two different fractions: "new" and "regenerated" (c.f. Dugdale, 1967). Nitrate is supplied at the bottom (300 m) by an infinite reservoir of constant concentration. At the surface, nitrate is supplied at a constant rate. "Regenerated" nitrogen (ammonia recycling) is originated from the excretion of heterotrophs and zooplankton. The overall system is assumed to reach a steady state; i.e., the output of particulate sinking material must equal the nitrate supply.

Several important differences exist between this model and the previous studies (e.g., Walsh, 1975; Wroblewski and O'Brien, 1976; Jamart *et al.*, 1977; Kiefer and Kremer, 1981) arise. First of all, two types of phytoplankton (based on size) with dissimilar uptake, growth rates and grazing processes are distinguished. Heterotrophic processes that provide a link between primary producers and higher levels of the trophic web are also considered. This last point was one of the major criticism advanced by several authors (e.g., Jamart *et al.*, 1977) to Wroblewski and O'Brien's type of models where the relationship between phytoplankton and zooplankton was

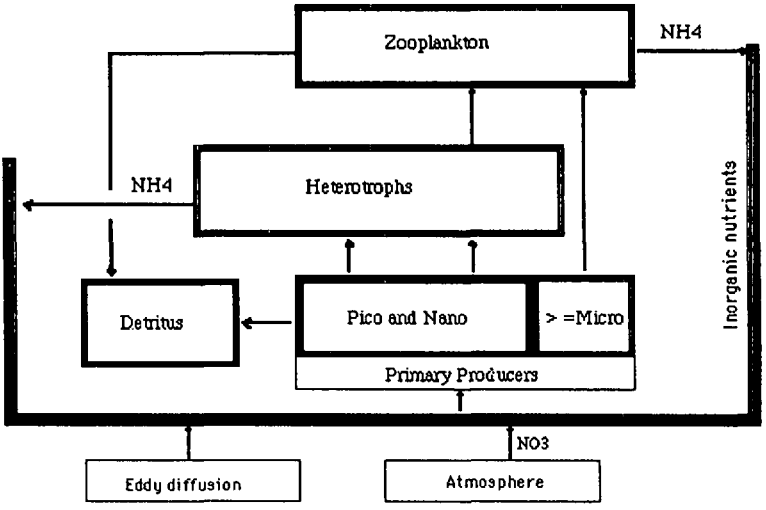

Figure 1. Biological model scheme (modified from the "classical" trophic food web of Michaels and Silver, 1988). Five state variables are considered: phytoplankton (two size fractions), heterotrophs and inorganic nutrients (nitrate and ammonia). Zooplankton and detritus are calculated but not modelled explicitly. Nitrate is provided to the system by eddy diffusion and the atmosphere, while ammonia is taken up by phytoplankton and returned to the system by heterotrophs and zooplankton excretion.

not adequately given. Finally, a detailed vertical frame provided by the physical model was included, and an atmospheric nitrate source that might be significant in the oligotrophic regions simulated (NW Mediterranean and Sargasso Sea) was also considered.

The general equations describing the distribution of the non-conservative variables in the one-dimensional biological model are in essence similar to previous studies (e.g., Wroblewski and O'Brien, 1976; Jamart *et al.*, 1977):

$$\begin{aligned}
\frac{\partial NO_3}{\partial t} &= \frac{\partial}{\partial z}\left[\lambda \frac{\partial NO_3}{\partial z}\right] - U_{NO_3L} - U_{NO_3P} \\
\frac{\partial NH_4}{\partial t} &= \frac{\partial}{\partial z}\left[\lambda \frac{\partial NH_4}{\partial z}\right] - U_{NH_4L} - U_{NH_4P} + \psi_Z + \psi_H \\
\frac{\partial L}{\partial t} &= \frac{\partial}{\partial z}\left[\lambda \frac{\partial L}{\partial z}\right] - s_1 + U_{NO_3L} + U_{NH_4L} - G_{ZL} \\
\frac{\partial P}{\partial t} &= \frac{\partial}{\partial z}\left[\lambda \frac{\partial P}{\partial z}\right] - s_2 U_{NO_3P} + U_{NH_4P} - G_{HP} \\
\frac{\partial H}{\partial t} &= \frac{\partial}{\partial z}\left[\lambda \frac{\partial H}{\partial z}\right] - s_3 + G_{HP} - G_{ZH} - \psi_H
\end{aligned} \tag{18–22}$$

where U is uptake, ψ is ammonia excretion and G is grazing. s_1, s_2 and s_3 are the sinking terms:

$$s_1 = v_1 \frac{\partial L}{\partial z}, \qquad s_2 = v_2 \frac{\partial P}{\partial z}, \qquad s_3 = v_3 \frac{\partial H}{\partial z}$$

where v_1, v_2 and v_3 are the vertical sinking velocities. These terms were included to simulate the sinking process of both phytoplankton sizes and heterotrophs state variables.

It is generally assumed that the phytoplankton growth is dependent on the light and nutrient regimes. However, there are important differences among modellers on how to represent the light-phytoplankton and nutrient-phytoplankton response. There is also no general agreement on whether the phytoplankton growth is influenced by those factors in an exclusive (e.g., Walsh, 1975) or multiplicative way (e.g. Wroblewski and O'Brien, 1976). In this model the assumption is made that a single factor is limiting at a time (Liebig's law), implying a choice between the light (ALIGHT) and the total nitrogen (ANUT) terms.

The nitrogen limitation term for each nutrient and size fraction was computed in the classical hyperbolic way (Walsh, 1975; Wroblewski and O'Brien, 1976) but different half-saturation constants were used for ammonia (ANH_4) and nitrate (ANO_3) uptake. ANO_3 and ANH_4 are added together for each phytoplankton size class to compute the total nitrogen uptake. As a result, this limitation factor could be greater than one, and then a proportional factor (nutrient uptake/total uptake) was introduced in the growth equations:

$$U_{NO_3L} = VMAX_L \cdot L \cdot \min(\text{ALIGHT}, \text{ANUT}) \cdot \frac{ANO_3}{ANUT} \tag{23}$$

$$U_{NO_3P} = VMAX_P \cdot P \cdot \min(\text{ALIGHT}, \text{ANUT}) \cdot \frac{ANO_3}{ANUT} \tag{24}$$

$$U_{NH_4P} = VMAX_P \cdot P \cdot \min(\text{ALIGHT}, \text{ANUT}) \cdot \frac{ANH_4}{ANUT} \tag{25}$$

$$U_{NH_4L} = VMAX_L \cdot L \cdot \min(\text{ALIGHT}, \text{ANUT}) \cdot \frac{ANH_4}{ANUT} \tag{26}$$

where the $VMAX$ terms are the maximum growth rates (t^{-1}) of each size, the ANx' terms, ALIGHT and min function have the form:

$$ANO_3 = \frac{[NO_3]}{k_{NO_3} + [NO_3]} e^{\Psi[NH_4]} \tag{27}$$

$$\mathrm{ANH_4} = \frac{[\mathrm{NH_4}]}{k_{\mathrm{NH_4}} + [\mathrm{NH_4}]} \tag{28}$$

$$\mathrm{ANUT} = \mathrm{ANO_3} + \mathrm{ANH_4} \tag{29}$$

$$\mathrm{ALIGHT} = \left(\frac{I_z}{k_l + I_z}\right) \tag{30}$$

where $k_{\mathrm{NO_3}}$, $k_{\mathrm{NH_4}}$ and k_l are the half saturation constants for nitrate, ammonia and light. and Ψ is a parameter related to the nitrate inhibition by ammonia concentration (Wroblewski and O'Brien, 1976). Light attenuation (I_z) at every depth was computed following the Beer-Lambert law:

$$I_z = I_0 e^{-(k_w + k_c + k_d)z} \tag{31}$$

where

I_0 is the surface incident light;
k_w is the pure water extinction, taken to be 0.03 $\mathrm{m^{-1}}$ (Kirk, 1983);
k_c is the extinction due to chlorophyll, computed as a lineal function of the chlorophyll *a* concentration (k_c = 0.03 Chl, Kirk, 1983);
k_d is the extinction due to several other factors (gilvin, particulate organic matter, etc.) characteristic of the region considered.

The grazing rate (G) is obtained for each state variable from simple hyperbolic equations of the form:

$$G_{HP} = G_{\max(p)} H \frac{P}{k_{grz(p)} + P} \tag{32}$$

$$G_{ZL} = G_{\max(z)} Z \frac{L}{k_{grz(z)} + L} \tag{33}$$

where $G_{\max(x)}$ are the maximum grazing rates (t^{-1}), Z the zooplankton in μmol N l^{-1} and $k_{grz(x)}$ are parameters.

Finally, zooplankton and heterotrophs excretion is assumed to be proportional to the biomass:

$$\Psi_Z = \epsilon \cdot Z \tag{34}$$

$$\Psi_H = \eta \cdot H \tag{35}$$

where ϵ and η are constants (t^{-1}).

b. Initial conditions. The initial conditions for the primary producers are a constant linear profile for each size class. These profiles are transformed in nitrogen units to be used by the model, and back to chlorophyll *a* in the model output. For this purpose, a linear regression was fitted to the data obtained by (Hollibaugh *et al.*, 1980; Ward *et al.*, 1989, see Fig. 2).

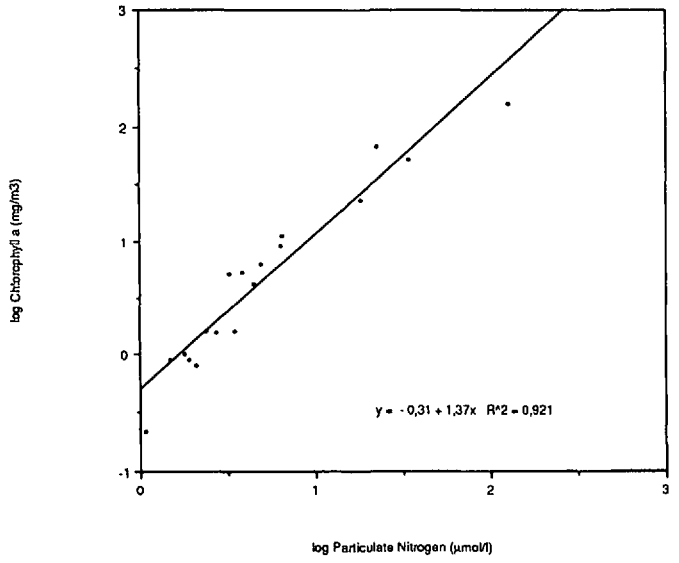

Figure 2. Linear equation obtained from bibliographic data for particulate nitrogen and chlorophyll *a*.

Initial conditions for nitrate and ammonia are also constant linear profiles. Heterotrophs are initially considered as the 60% of the total small primary producers (pico and nanoplankton, Michaels and Silver 1988), zooplankton is initialized as a proportion of large phytoplankton and heterotrophs added together and *POM* is initially set to zero:

$$Z^z_{t=0} = (G^z_{t=0} + H^z_{t=0}) \cdot k$$

$$H^z_{t=0} = 0.6P^z_{t=0}$$

$$POM^z_{t=0} = 0$$

Since our purpose is to reach an equilibrium between the particulate flux going down and the nitrate supply, initial condition values affect the time needed to attain this equilibrium but not the final results.

c. Boundary conditions. With the exception of nitrate, no fluxes at the surface are allowed:

$$\lambda \frac{\partial P}{\partial z}\bigg|_{z=0} = \lambda \frac{\partial L}{\partial z}\bigg|_{z=0} = \lambda \frac{\partial G}{\partial z}\bigg|_{z=0} = \lambda \frac{\partial H}{\partial z}\bigg|_{z=0} = \lambda \frac{\partial \mathrm{NH_4}}{\partial z}\bigg|_{z=0} = 0$$

$$\lambda \frac{\partial \mathrm{NO_3}}{\partial z} = j_{\mathrm{NO_3}}$$

where j_{NO_3} (μM N-NO_3 l^{-1} s^{-1}) is the atmospheric nitrate supply to the system.

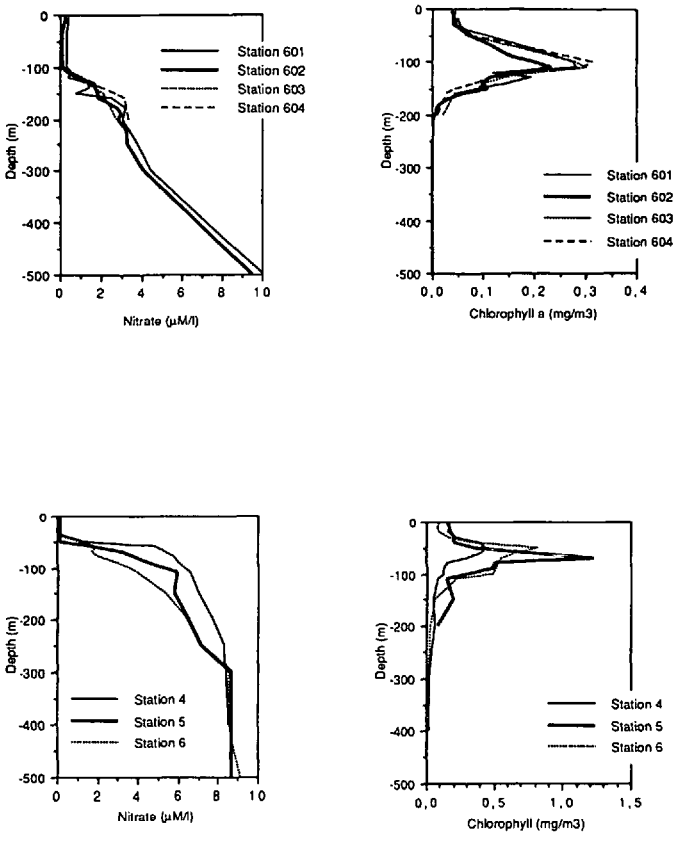

Figure 3. Nitrate and chlorophyll profiles observed for the SW Sargasso Sea (September 1987, top line) and NW Mediterranean (May 1987, bottom line). Only the top 500 m are represented.

At the bottom (z = 300 m) an infinite nitrate reservoir is assumed. No fluxes for ammonia, primary producers and heterotrophs are allowed.

For the diffusion equation we used the same algorithm described in the physical model, while the biological terms were treated explicitly. The time step used was 1 hour, and the grid size and spacing were the same as in the physical model.

4. Model validation and data sets

Validation of model results was carried out using data from two stations sampled repetitively over several days in the western Mediterranean (Masó and Grup PEPS, 1988) and the Sargasso Sea (Varela and Cruzado, 1988; Neveux, 1988). For completeness, a brief description of the data available is presented (Fig. 3). Detailed description of the methods used for all the variables can be found in the above references.

Samples from the Sargasso Sea were collected during September–October 1987 at 10 different locations near 61W and between 30 and 31N. Each station was repeatedly sampled during the same day by series of CTD casts with a rosette attached. Samples for nutrient and chlorophyll were analyzed using an autoanalyzer and standard techniques. Data from the western Mediterranean (2–4E and 40–41N) come from a series of cruises carried out onboard the R/V García del Cid between 1985 and 1987. The samples were taken with 5 l Niskin bottles from where nutrient and chlorophyll data were obtained.

5. Results

a. Physical and biological model, real conditions. The combined physical and biological model was run using real wind, nutrient and biological data from the Sargasso Sea and the Western Mediterranean Sea.

In order to compare simulations with data, the following procedure was used: First, the physical model was initialized with real temperature, and salinity taken from CTD casts. Wind strength and direction was obtained at the vessel's bridge at the same station. The physical model was run and its output compared with data from the time-following CTD cast at the same location. The eddy diffusion coefficients obtained in the physical model were then used to initialize the biological model. Finally, output from the biological model was compared with nitrate and chlorophyll data sampled at the latter station.

Integration of the equations in the biological model was continued until the integrated flux of particulate material going out from the system equated the nitrate supply. This assumption makes the model integration times strongly dependent on the initial conditions of the state variables.

Table 1 shows the values given to the parameters used, which were held constant for the two places, except those concerning light extinction (higher values in the western Mediterranean Sea) and grazing parameterization.

The thermocline and eddy diffusion evolution for the Sargasso Sea are shown in Figure 4a and 4b. During the first hours the mixed layer deepens and the surface temperature reduces by about 0.3°C. After the first 8 hours no significant changes are observed. The eddy diffusion coefficient increases sharply just below the sea surface to about 200 $cm^2\ s^{-1}$, but strongly decreases below 20 m depth.

In the western Mediterranean Sea, results are somewhat similar (Fig. 5a and 5b), but the mixed layer depth is slightly greater. We also find the same pattern in the eddy diffusion vertical distribution, with values dropping quickly below the thermocline.

Figure 6 shows that good agreement exists between observed and predicted temperature profiles for the Sargasso Sea. Data vary from near 28°C in the surface to about 19°C at 50 m depth. A good correspondence between observed and computed values is obtained, since the maximum difference account for not more than 0.5°C.

Table 1. Parameter set used in the calibration of the biological model for both areas. Since previous sensitivity tests showed the slight influence of the sinking velocity w_x, these parameters were set to zero.

Parameter name	Sargasso Sea	Catalan Sea
Incident light	800 $\mu E\ m^{-2}\ d^{-1}$	800 $\mu E\ m^{-2}\ d^{-1}$
Light extinction	0.05 m^{-1}	0.06 m^{-1}
$VMAX_P$	$2 \times 10^{-5}\ seg^{-1}$	$2 \times 10^{-5}\ seg^{-1}$
$VMAX_L$	$1 \times 10^{-5}\ seg^{-1}$	$1 \times 10^{-5}\ seg^{-1}$
KNO_{3L}	0.15 $\mu mol\ NO_3\ l^{-1}$	0.15 $\mu mol\ NO_3\ l^{-1}$
KNO_{3P}	0.05 $\mu mol\ NO_3\ l^{-1}$	0.05 $\mu mol\ NO_3\ l^{-1}$
KNH_{4L}	0.2 $\mu mol\ NH_4\ l^{-1}$	0.2 $\mu mol\ NH_4\ l^{-1}$
KNH_{4P}	0.1 $\mu mol\ NH_4\ l^{-1}$	0.1 $\mu mol\ NH_4\ l^{-1}$
G_{ZL}	$5.3 \times 10^{-6}\ seg^{-1}$	$1.5 \times 10^{-6}\ seg^{-1}$
G_{ZH}	$7.1 \times 10^{-6}\ seg^{-1}$	$2.0 \times 10^{-6}\ seg^{-1}$
G_{HP}	$2.6 \times 10^{-6}\ seg^{-1}$	$6.0 \times 10^{-7}\ seg^{-1}$
ψH	$2.5 \times 10^{-3}\ seg^{-1}$	$2.5 \times 10^{-3}\ seg^{-1}$
ψZ	$6.7 \times 10^{-3}\ seg^{-1}$	$6.7 \times 10^{-3}\ seg^{-1}$

Using the eddy diffusion values provided by the mixed layer submodel, the biological submodel was run in the two locations. In the Sargasso Sea the corresponding observed and predicted vertical profiles for nitrate and total chlorophyll *a* are showed in Figure 7a and 7b. The nutricline depth is correctly simulated, while the overall nitrate predicted profile is somewhat lower than the observed. The DCM depth and magnitude are adequately simulated, but chlorophyll values in the deeper 50 m are slightly larger.

A similar trend is observed in the western Mediterranean simulation (Fig. 8a and 8b), but with higher chlorophyll values, shallower nitracline and larger nitrate values at 300 m depth. The DCM depth, magnitude and deep values are reproduced quite exactly. At the surface, however, predicted values differ from the observed in about 0.1 mg m^{-3} and there is still a nitrate deficiency in the predicted values, particularly below 100 m.

6. Discussion

The present work shows that the vertical chlorophyll structure in oligotrophic temperate areas can be well reproduced by means of coupled physical/biological models.

Oligotrophic systems are largely dependent on hydrodynamic processes (mainly eddy diffusion and internal waves) to obtain the nutrients required for primary production. This circumstance is reflected in the Figure 9 where the biological submodel output for several different profiles of eddy diffusion (λ) is shown. Increasing λ in the upper layer leads to more homogeneous chlorophyll distribution

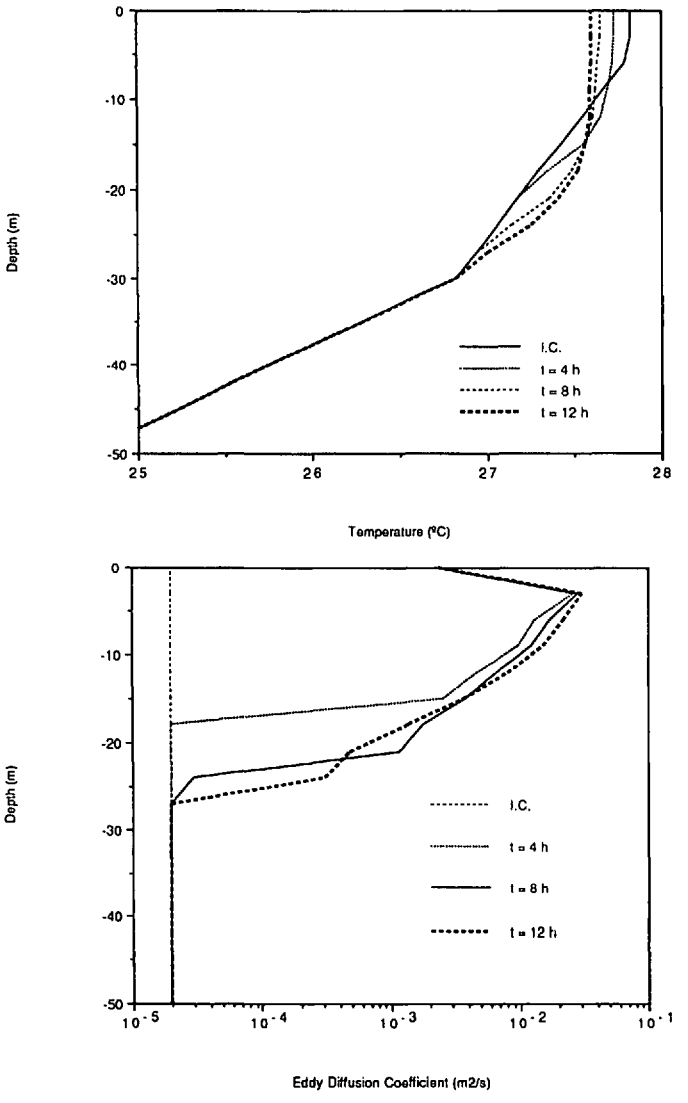

Figure 4. (a) Temperature evolution obtained with the physical model using real wind, temperature and salinity data for the Sargasso Sea at different integration times. I.C. means initial conditions, and only the top 50 m are represented. (b) Eddy diffusion evolution obtained with the physical model using real wind, temperature and salinity data for the Sargasso Sea at different integration times.

in this layer, while increasing λ values below the thermocline enhances nutrient flux from downward, and thus producing a larger and shallower chlorophyll maximum.

A sensitivity analysis showed that the use of different vertical eddy diffusion coefficients can be of great help in reproducing the DCM over the year. A constant

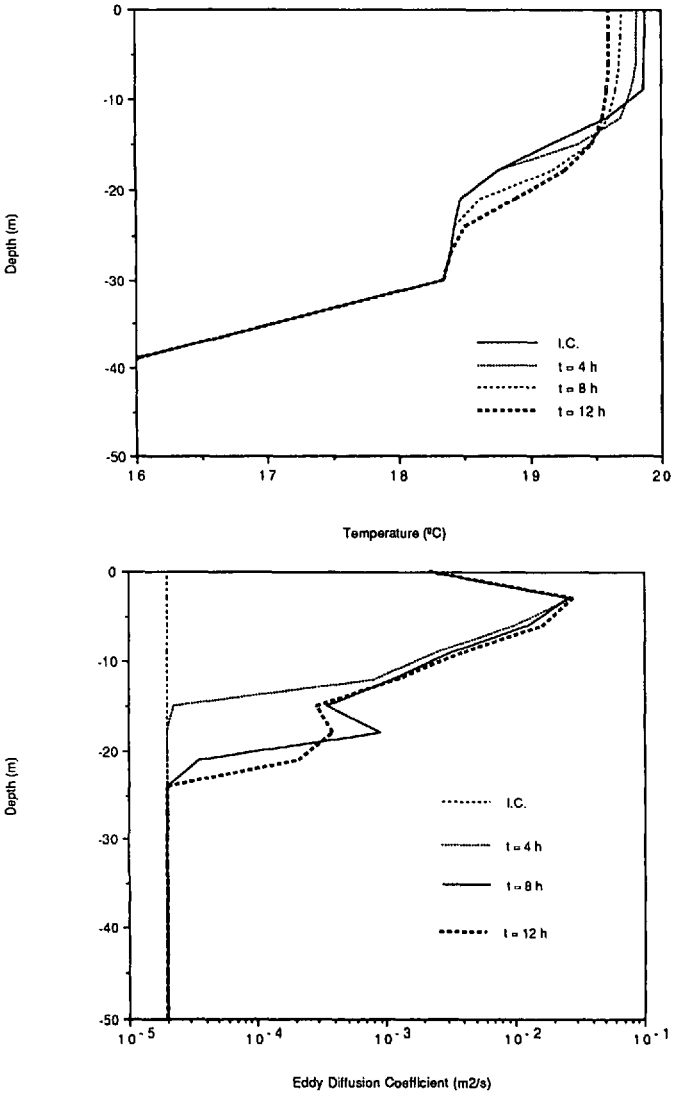

Figure 5. (a) Temperature evolution obtained with the physical model using real wind, temperature and salinity data for the Mediterranean Sea at different integration times. I.C. means initial conditions, and only the top 50 m are represented. (b) Eddy diffusion evolution obtained with the physical model using real wind, temperature and salinity data for the Mediterranean Sea at different integration times.

and relatively larger λ (e.g., typical of a winter situation) of 1–2 $cm^2\ s^{-1}$ in the top 100 or 150 m forces a more linear nutrient distribution in this layer, and thus a more vertically uniform chlorophyll profile. If this eddy diffusion coefficient is large enough, the chlorophyll maximum can be found at the surface. On the other hand, relatively larger λ's near the surface but exponentially decreasing below the thermo-

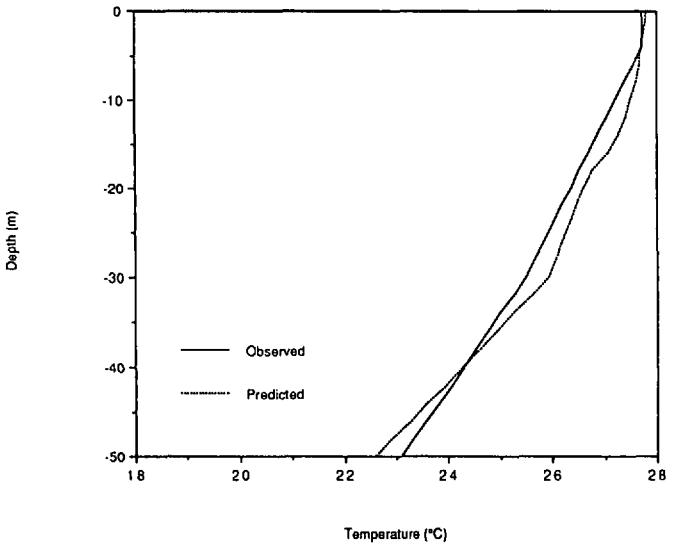

Figure 6. Observed and predicted temperature profiles using real wind, temperature and salinity data (SW Sargasso Sea, September 1987). The solid line represents the CTD data, while the dashed line is the simulated profile as predicted by the physical model after 12 hs of simulation.

cline could substantially reduce the amount of nutrient that reach the ocean upper layer and, helped by the organisms' uptake, produce a chlorophyll profile typical of stratified waters.

The one-dimensional mixed layer model used provides good eddy diffusion estimates above the thermocline, but estimates are too low below the thermocline and inconsistent with values provided by field experiments (Rooth and Ostlund, 1972; Kiefer *et al,* 1976; Bienfang and Gunderson, 1977). One may correct these values by filtering high frequency phenomena like internal waves and double diffusion (Wang, 1982; 1984) or including the complex physics involved in those processes.

An alternative and simpler approach allow to determine if the vertical eddy diffusion coefficient is underestimated by not including the double diffusion effects (Hamilton *et al,* 1989):

$$\frac{K_{S,f}}{K_{S,t}} = \frac{(R_\rho^{-1} - 1)}{0.265(1 - \gamma_{\text{Stern}})} \tag{36}$$

where $K_{S,f}$ is eddy diffusion including double diffusion effects, s is eddy diffusion without these effects, R_ρ is the constant density ratio and γ_{Stern} is the flux ratio (Stern, 1976; Kunze, 1987).

Hamilton's formula was computed in the physical model and the results suggest that in some points below the thermocline the k-model underestimated the turbulent

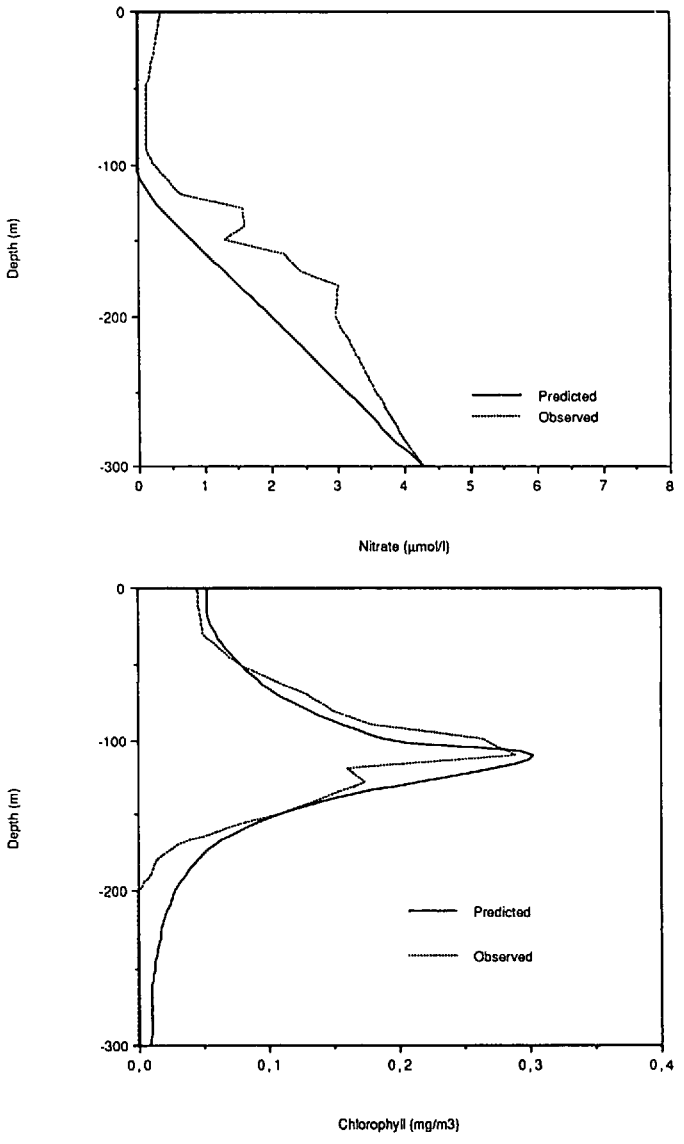

Figure 7. (a) Observed and predicted nitrate profiles (SW Sargasso Sea, September 1987). The solid line is the observed data, while the dashed line is the simulated profile obtained with the biological model at steady state conditions using the vertical eddy diffusion profile provided by the physical model. (b) Observed and predicted chlorophyll profiles (SW Sargasso Sea, September 1987). The solid line is the observed data, while the dashed line is the simulated profile obtained with the biological model as detailed in (a).

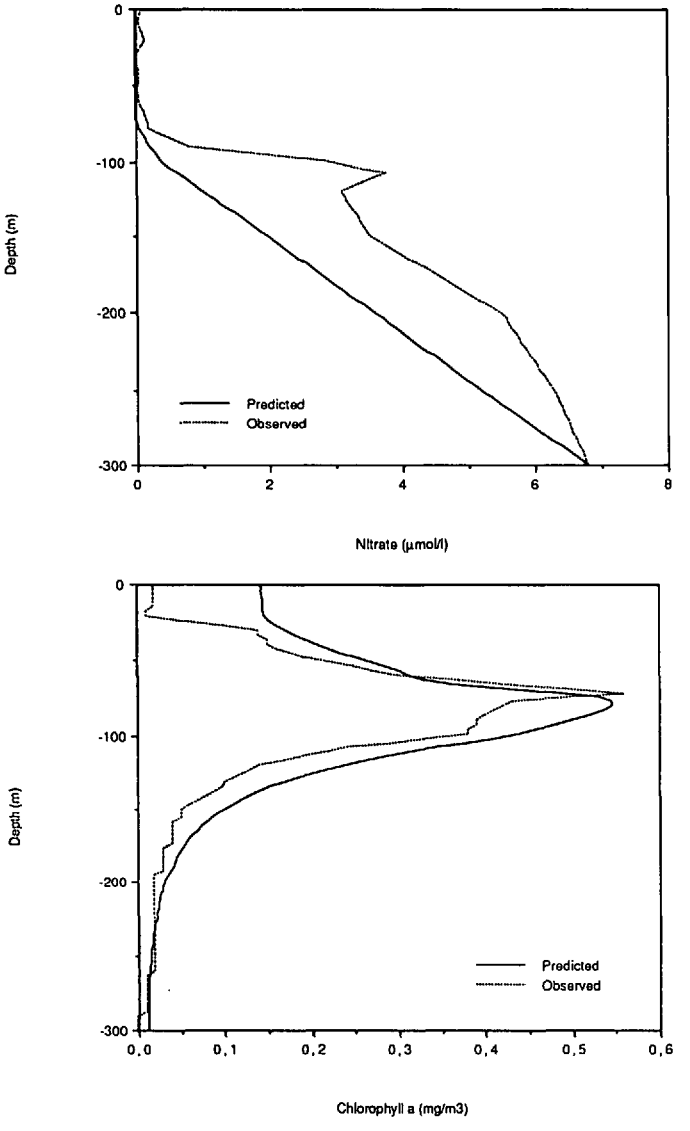

Figure 8. (a) Observed and predicted nitrate profiles (NW Mediterranean Sea, May 1987). The solid line is the observed data, while the dashed line is the simulated profile obtained with the biological model at steady state conditions using the vertical eddy diffusion profile provided by the physical model. (b) Observed and predicted chlorophyll profiles (NW Mediterranean Sea, May 1987). The solid line is the observed data, while the dashed line is the simulated profile obtained with the biological model as detailed in (a).

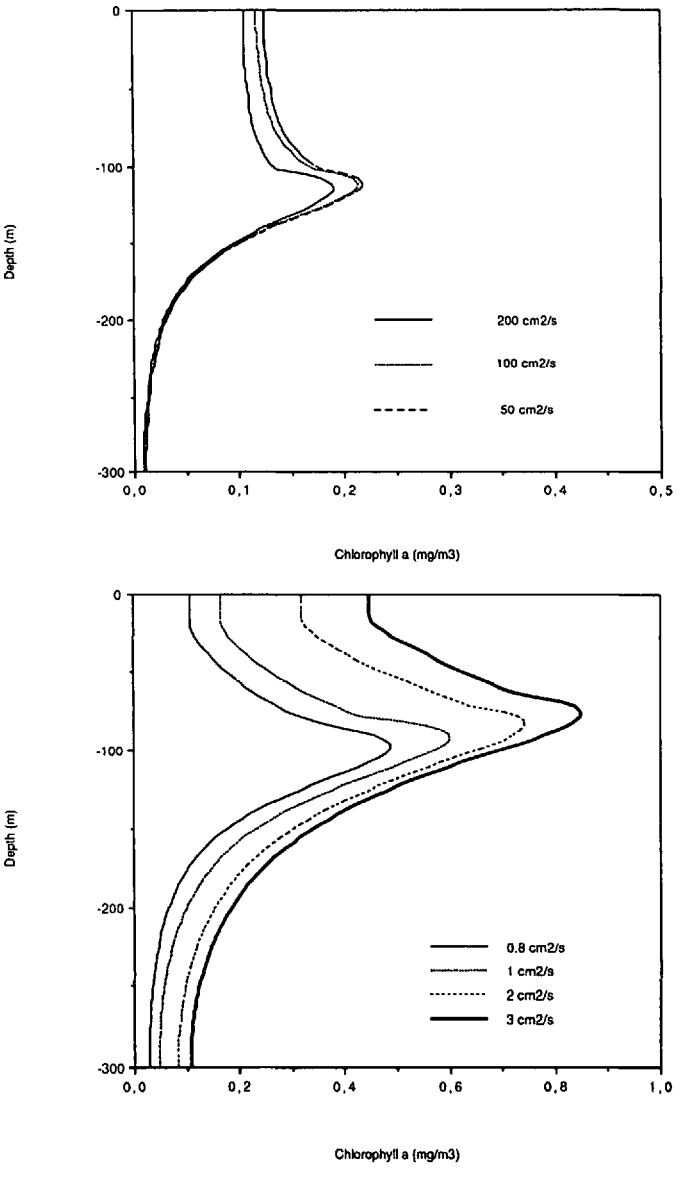

Figure 9. (a) Effect of using different eddy diffusion profiles above the thermocline on the vertical distribution of chlorophyll *a*. Each profile was set up with a different surface value and use the same exponential decrease to finally reach 0.2 $cm^2\ s^{-1}$. (b) Effect of using different eddy diffusion values below the thermocline on the vertical distribution of chlorophyll *a*.

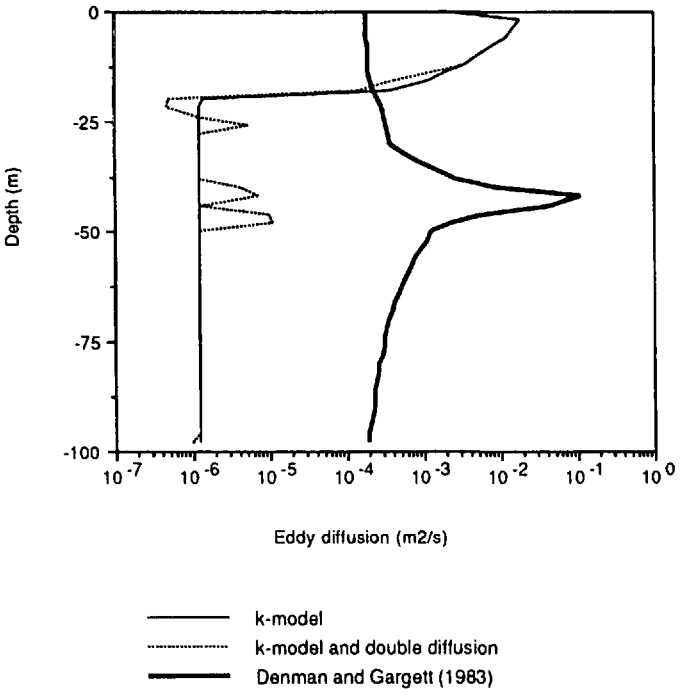

Figure 10. Eddy diffusion estimates with three different methods for the SW Sargasso Sea. The *k*-model (solid line) gives good estimates of the vertical eddy diffusion values above the thermocline, but below results are consistently low. Including the effects of double diffusion (Hamilton *et al.*, 1989, dotted line) still gives low λ values (see text). The Denman and Gargett (1983) formulae (dashed line) using temperature and salinity data and $\epsilon = 2 \times 10^{-8}$ m^2 s^{-3} provides useful estimates of the eddy diffusion below the thermocline.

diffusion values (Fig. 10). Hamilton's equation was insufficient to account for the above cited field experiment values but clearly enhanced nutrient fluxes in the water column. To get the observed values, a more complex three-dimensional physical model including the effect of internal waves is probably needed. This points to the importance of considering internal waves in the vertical distribution of phytoplankton (Holloway and Denman, 1989).

Another useful way to estimate turbulent diffusion coefficient providing the Brünt-Väisäla frequency (N^2) and the kinetic energy (E) is Denman and Gargett's (1983) equation, which is also included in Figure 10.

$$K_z = 0.25EN^2 \tag{37}$$

Denman and Gargett's (1983) formula provides useful eddy diffusion estimates below the thermocline, while results above are clearly misleading. As a consequence, the possibility of combining the physical submodel results above the thermocline with the Denman and Gargett's stability formulae below is appealing and effortless.

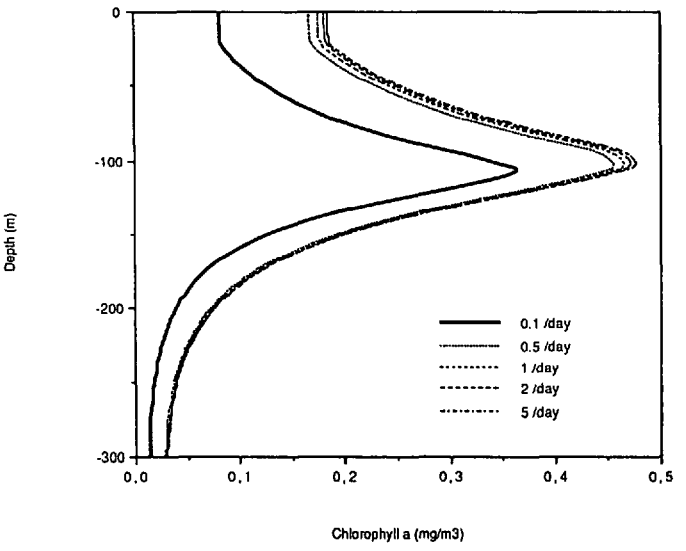

Figure 11. Effect of varying the maximum grazing rate on the vertical distribution of the total chlorophyll *a* in the water column. Only the heterotrophs grazing over small-size phytoplankton is represented.

7. Summary and conclusions

The physical/biological model described, although simulating a simplified trophic food web, has been demonstrated to have the main elements to reproduce adequately the deep chlorophyll maximum structure. An important point to consider is that the calibration parameters used are within the range published (Eppley *et al,* 1966; Eppley, 1972; Rhee and Gotham, 1981; Schelsinger *et al,* 1981; Banse, 1982 for the growth parameters; MacIsaac and Dugdale, 1969; Eppley, 1969 for the half saturation constants; Radach *et al,* 1984 for the grazing rates).

Sinking factors do not seem to affect the DCM structure and could then be neglected in a one-dimensional model of the DCM in those areas without losing a great amount of precision. This in effect considerably simplifies the equations and computations. Instead, at least an important fraction of phytoplankton is actively growing in low light levels and at the maximum nitrate gradient.

These results tend to support Kiefer and Kremer's (1981) stratigraphic hypothesis about the chlorophyll maximum structure. Moreover, sensitivity experiments showed that atmospheric nitrate inputs do not produce a significative enhancement of primary production at the DCM depth and also that grazing processes affect mainly the magnitude of the DCM but not its position in the water column (Fig. 11).

However, the DCM is a highly dynamical structure not only dependent on the phytoplankton growth and metabolic regulation, but also strongly sensitive to the light extinction (Fig. 12) and vertical eddy diffusion. As a consequence, the DCM is found at a depth determined by the nutrient flux from downwards and the light field

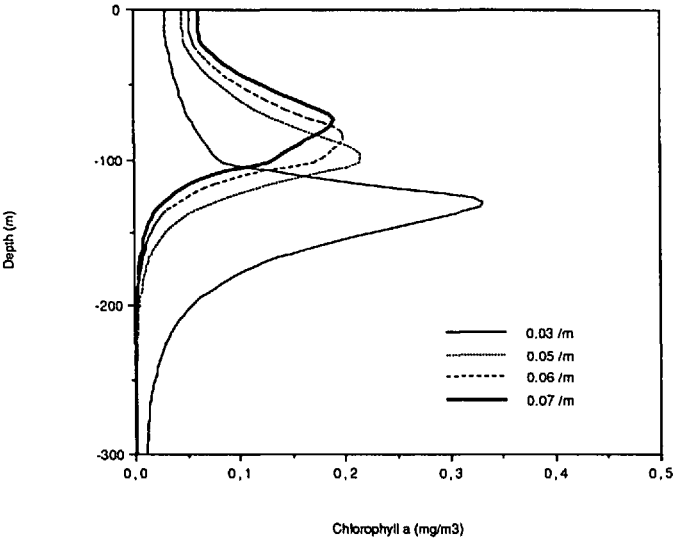

Figure 12. Effect of varying the total light extinction on the vertical distribution of the total chlorophyll *a* in the water column.

characteristics. This suggests the deep chlorophyll maximum to be the result of the new production, the regenerated production playing only a secondary role.

Acknowledgments. Partial support from the E.C. MAST Program under project EURO-MODEL (0043-C) and the FICITIB (SP1CE91-04) is gratefully acknowledged (J. T.). We are also particularly thankful to one of the referees, whose comments significantly improved the quality and readability of the manuscript.

REFERENCES

Anderson, G. C. 1969. Subsurface chlorophyll maximum in the Northeast Pacific Ocean. Limnol. Oceanogr., *14,* 386–391.

Banse, K. 1982. Cell volumes, maximal growth rates of unicellular algae and ciliates, and the role of ciliates in the marine pelagial. Limnol. Oceanogr., *27,* 1059–1071.

—— 1987. Clouds, deep chlorophyll maxima and the nutrient supply to the mixed layer of stratified water bodies. J. Plank. Res., *9,* 1031–1036.

Bienfang, P. K. and K. Gunderson. 1977. Light effects on nutrient limited, oceanic primary production. Mar. Biol., *43,* 187–191.

Chen, D., S. G. Horrigan and D. P. Wang. 1988. The late summer vertical nutrient mixing in Long Island Sound. J. Mar. Res., *46,* 753–770.

Denman, K. L. and A. E. Gargett. 1983. Time and space scales of vertical mixing and advection of phytoplankton in the upper ocean. Limnol. Oceanogr., *28,* 801–815.

Dugdale, R. C. 1967. Nutrient limitation in the sea: dynamics, identification, and significance. Limnol. Oceanogr., *12,* 685–695.

Eppley, R. W. 1972. Temperature and phytoplankton growth in the sea. Fish. Bull. US., *70,* 063–1085.

Eppley, R., J. Rogers and J. McCarthy. 1969. Half saturations constants for uptake of nitrate and ammonium by marine phytoplankton. Limnol. Oceanogr., *14,* 912–920.

Eppley, R. W. and P. R. Sloan. 1966. Growth rates of marine phytoplankton: correlation with light absorption by cell chlorophyll *a*. Phys. Plant, *19,* 47–59.

Estrada, M. and J. Salat. 1989. Phytoplankton assemblages of deep and surface water layers in a Mediterranean frontal zone. Scient. Mar., *53,* 203–214.

Flos, J and J. Tintoré. 1990. Summer frontal contribution to the fertilization of oceanic waters off the northeast Spanish coast. Oceanologica Acta, *13,* 21–30.

Gaspar, P., T. Gregoris, R. Stull and C. Boissier. 1988. Long-term simulations of upper ocean vertical mixing using models of different types *in* Small-scale Turbulence and Mixing in the Ocean, J. C. J. Nihoul, ed., Elsevier Science Publishers.

Gill, A. E. and J. S. Turner. 1976. A comparison of seasonal thermocline models with observations. Deep-Sea Res., *23,* 391–401.

Hamilton, J. H., M. R. Lewis, and B. R. Ruddick. 1989. Vertical fluxes of nitrate associated with salt fingers in the World's oceans. J. Geophys. Res., *94,* 2137–2145.

Herbland, A. 1983. Le maximum de chlorophylle dans l'Atlantique tropical oriental: description, ecologie, interpretation. Oceanogr. Trop., *18,* 295–318.

Hollibaugh, J., A. Carruthers, J. Fuhram and F. Azam. 1980: Cycling of organic nitrogen in marine plankton communities studied in enclosed water columns. Mar. Biol. *59,* 15–21.

Holloway, G. and K. Denman. 1989. Influence of internal waves on primary production. J. Plank. Res., *11,* 409–413.

Jamart, B. M., D. F. Winter, K. Banse, G. C. Anderson and R. K. Lam. 1977. A theoretical study of phytoplankton growth and nutrient distribution in the Pacific Ocean off the northwestern U.S. coast. Deep-Sea Res., *24,* 753–773.

Kiefer, D. A. and J. N. Kremer. 1981. Origins of vertical patterns of phytoplankton and nutrients in the temperate, open ocean: a stratigraphic hypothesis. Deep-Sea Res., *28A,* 1087–1105.

Kiefer, D. A., R. J. Olson and O. Holm-Hansen. 1976. Another look at the nitrite and chlorophyll maxima in the Central North Pacific. Deep-Sea Res., *23,* 1199–1208.

Kirk, J. T. O. 1983. Light and Photosynthesis in Aquatic Ecosystems. Cambridge University Press, Cambridge, 401 pp.

Klein, P. and B. Coste. 1984. Effects of wind-stress variability and nutrient transport into the mixed layer. Deep-Sea Res., *31,* 21–37.

Kunze, E. 1987. Limits on growing, finite-length salt fingers: a Richardson number constraint. J. Mar. Res., *45,* 533–556.

MacIsaac, J. and R. C. Dugdale. 1969. The kinetics of nitrate and ammonia uptake by natural populations of marine phytoplankton. Deep-Sea Res., *16,* 45–57.

Masó, M. and Grup PEPS. 1988. Datos oceanográficos básicos de las campañas FRONTS-3-85, FRONTS-6-85, PEP-86, FRONTS-11-86 y PEP-87 en el Mar Catalán. Institut de Ciencies del Mar de Barcelona (CSIC).

Mellor, G. L. and T. Yamada. 1974. A hierarchy of turbulence closure models for planetary boundary layers. J. Atmos. Sci., *31,* 1791–1806.

Michaels, A. F. and M. W. Silver, 1988. Primary production, sinking fluxes and the microbial food web. Deep-Sea Res., *35,* 473–490.

Millero, F. and A. Poisson. 1981. International one-atmosphere equation of state of seawater. Deep-Sea Res., *28A,* 625–629.

Neveux, J. CHLOMAX Rapport Campagne á la Mer. Greco P4, September 14 to October 13.

Nihoul, J. C. J. 1982. Oceanography of semi-enclosed seas *in* Hydrodynamics of Semi-Enclosed Seas, J. C. J. Nihoul, ed., Elsevier Publ. Amsterdam, 1–12.

Radach, G., J. Berg, B. Heinemann, and M. Krause. 1984. On the relation of primary production to grazing during the Fladen ground experiment 1976. *in* Flows of Energy and Materials in Marine Ecosystems, M. J. R. Fasham, ed., Nato Conference Series IV. Vol. 13, Plenum Press, New York, 597–625.

Rhee, G. and I. Gotham. 1981. The effect of environmental factors on phytoplankton growth. Light and the interactions of light with nitrate. Limnol. Oceanogr., *26,* 649–659.

Riley, G. A. 1949. Quantitative ecology of the plankton of the western North Atlantic. Bull Bingham Oceanographic Collection, *12,* 1–169.

Rodi, W. 1987. Examples of calculations methods for flow and mixing in stratified fluids. J. Geophys. Res., *92,* 5305–5328.

Rooth, C. G. and H. G. Ostlund. 1972. Penetration of tritium into the Atlantic thermocline. Deep-Sea Res., *19,* 481–492.

Schelsinger, D. A., L. A. Molot, and B. J. Shuter. 1981. Specific growth rates of freshwater algae in relation to cell size and light intensity. Can. J. Fish. Aquat. Sci. 38, 1052–1058.

Steele, J. H. and C. S. Yentsch. 1960. The vertical distribution of chlorophyll. J. Mar. Biol. Ass. U.K. 39, 217–226.

Stern, M. 1976. Maximum buoyancy flux across a salt finger interface. J. Mar. Res, *34,* 95–110.

Taguchi, S., G. R. Ditullio, and E. A. Laws. 1988. Physiological characteristics and production of mixed layer and chlorophyll maximum phytoplankton populations in the Caribbean Sea and western Atlantic Ocean. Deep-Sea Res., *35,* 1363–1377.

Takahashi, M. and T. Hori. 1984. Abundance of picophytoplankton in the subsurface chlorophyll maximum layer in subtropical and tropical waters. Mar. Biol., *79,* 177–186.

Varela, R. A. and A. Cruzado. 1988. Chlomax Technical Report. Centre d'Éstudis Avançats de Blanes, (CSIC), 140 pp.

Walsh, J. J. 1975. A spatial simulation model of the Peru upwelling ecosystem. Deep-Sea Res., *22,* 201–236.

Wang, D. P. 1982. Development of a three dimensional, limited-area (Island) shelf circulation model. J. Phys. Oceanogr., *12,* 1191–1199.

—— 1984. Mutual intrusion of a gravity current and density front formation. J. Phys. Oceanogr, *14,* 1191–1199.

Ward, B. B., K. A. Kilpatrick, E. H. Renger, and R. W. Eppley. 1989. Biological nitrogen cycling in the nitracline. Limnol. Oceanogr., *34,* 493–513.

Wroblewski, J. S. and J. O'Brien. 1976. A spatial model of phytoplankton patchiness. Mar. Biol., *35,* 161–175.

Received: *15 August, 1991;* revised: *7 April, 1992.*